

Tropopause-Penetrating Convection from Three-Dimensional Gridded NEXRAD Data

DAVID L. SOLOMON AND KENNETH P. BOWMAN

Department of Atmospheric Sciences, Texas A&M University, College Station, Texas

CAMERON R. HOMEYER

School of Meteorology, University of Oklahoma, Norman, Oklahoma

(Manuscript received 13 July 2015, in final form 13 November 2015)

ABSTRACT

A new method that combines radar reflectivities from individual Next Generation Weather Radars (NEXRAD) into a three-dimensional composite with high horizontal and vertical resolution is used to estimate storm-top altitudes for the continental United States east of the Rocky Mountains. Echo-top altitudes are compared with the altitude of the lapse-rate tropopause calculated from the ERA-Interim reanalysis and radiosondes. To sample the diurnal and annual cycles, tropopause-penetrating convection is analyzed at 3-h intervals throughout 2004. Overshooting convection is most common in the north-central part of the United States (the high plains). There is a pronounced seasonal cycle; the majority of overshooting systems occur during the warm season (March–August). There is also a strong diurnal cycle, with maximum overshooting occurring near 0000 UTC. The overshooting volume decreases rapidly with height above the tropopause. Radiosonde observations are used to evaluate the quality of the reanalysis tropopause altitudes and the dependence of overshooting depth on environmental characteristics. The radar–radiosonde comparison reveals that overshooting is deeper in double-tropopause environments and increases as the stability of the lower stratosphere decreases.

1. Introduction

Changes in the composition of the upper troposphere and lower stratosphere (UTLS) have been shown to have large impacts on the chemistry, climate, and radiation budget of the troposphere and stratosphere (Holton et al. 1995; Stohl et al. 2003; Forster et al. 2007; Gettelman et al. 2011). Because the lifetimes of many trace constituents are long in the UTLS, transport is often the dominant factor affecting their distributions. Many previous studies focusing on stratosphere–troposphere exchange (STE) have investigated processes such as Rossby wave breaking, the Brewer–Dobson circulation, and tropopause folding as pathways for transport across the tropopause. There is a relatively good understanding of the dynamics and chemistry of these large-scale processes, but transport by smaller-scale

processes, including convection, has not been studied as extensively.

Deep convection occurs in many locations around the globe and has the potential to lift boundary layer and lower tropospheric air rapidly into the UTLS. This study focuses on assessing the importance of tropopause-penetrating convection as a source of air in the lower stratosphere. Therefore, we are interested primarily in troposphere-to-stratosphere transport (TST), following the nomenclature of Stohl et al. (2003). Studies of convection in the tropics have shown that convection does occur up to the altitude of the tropopause, and it plays a key role in determining the abundance of trace species entering the stratosphere (Alcala and Dessler 2002; Gettelman et al. 2002; Dessler 2002). Numerous studies have also shown evidence of convection affecting the extratropical UTLS (e.g., Dickerson et al. 1987; Poulida et al. 1996; Fischer et al. 2003; Fromm and Servranckx 2003; Hegglin et al. 2004; Ray et al. 2004; Hanisco et al. 2007; Anderson et al. 2012; Homeyer et al. 2014b). Many of these previous studies of convective STE focus on individual events or a small number of case studies.

Corresponding author address: Kenneth P. Bowman, 3150 TAMU, Dept. of Atmospheric Sciences, Texas A&M University, College Station, TX 77843-3150.
E-mail: k-bowman@tamu.edu

More recently, model simulations of extratropical convection and the associated transport have been carried out (e.g., Gray 2003; Wang 2003; Mullendore et al. 2005; Chagnon and Gray 2010; Homeyer et al. 2014a; Bigelbach et al. 2014). These modeling studies, and the observational studies mentioned above, show that deep convection can penetrate through the tropopause and influence the composition of the lower stratosphere. Because many of these simulations focus on a small number of storms, they are useful for diagnosing the impact of individual systems, but they cannot quantify the regional or global impacts of deep convection on the layer. On the other hand, global models with parameterized convection do not resolve individual convective cells, so the total impact of convection on the lower stratosphere through TST is difficult to assess.

Several studies have attempted to use satellite observations to quantify the frequency and location of deep convection that penetrates the tropopause with varying success. Berendes et al. (2008) use a combination of visible and near-IR texture and reflectance to objectively detect convection penetrating the tropopause. This technique performs well at times around solar noon, but it suffers at larger solar zenith angles as a result of enhanced texture in the visible channel imagery during these times, and it cannot be used at night when continental convection typically reaches its maximum intensity (Dai et al. 1999). Lindsey and Grasso (2008) and Rosenfeld et al. (2008) use near-IR reflectance and ice particle effective radius techniques to locate storms that have penetrated the tropopause, but their method suffers from some of the same diurnal cycle issues as above, making these techniques less than ideal for a complete accounting of overshooting systems (Bedka et al. 2010).

Other studies have used a technique that employs the difference between 6–7- μm water vapor absorption and ~11- μm infrared window channel brightness temperature for overshooting convection detection (e.g., Fritz and Laszlo 1993; Ackerman 1996; Schmetz et al. 1997; Setvák et al. 2007; Martin et al. 2008). This technique works when the lapse rate in the stratosphere is inverted, and the environmental temperatures increase with height. If water vapor is present above the storm tops, either by being injected into the lower stratosphere by the storms themselves, or by being advected from elsewhere, it emits at the warmer stratospheric temperature while the emissions in the infrared window channel come from the colder cloud top. The difference between these two sources can then be used to diagnose where overshooting is occurring. The difference threshold needed for overshoot detection with this method varies depending on the measuring platform used, stratospheric

lapse rate, intensity of the updraft, and residence time of the water vapor in the stratosphere. When one of the two conditions above is not met, the method will not work (Setvák et al. 2013).

Bedka et al. (2010) use a combination of infrared window brightness temperature spatial gradients and Global Forecast System (GFS) 6-h forecasts of tropopause temperature to create a 5-yr climatology of overshooting convection across the eastern portion of the United States. This method provides a representation of total overshooting convection by locating “cold” pixels with infrared window brightness temperatures less than or equal to 215 K and identifies the corresponding tropopause temperatures at each location. The mean anvil temperature surrounding each pixel is then calculated and if the cold pixel is at least 6.5 K colder than the anvil it is considered to be overshooting. Bedka et al. (2010) estimate that the pixels they identify as overshooting are at least 0.7–0.9 km above the surrounding anvil cloud, assuming typical lapse rates of overshooting storms (Negri 1982; Adler et al. 1983), and find the largest number of overshooting occurrences occur across the southeastern United States and southern Great Plains. The biggest drawback to this method is that overshooting height is inferred from analyzed temperature profiles, which can be, for example, isothermal just above the tropopause. Furthermore, the large-scale analyses do not account for diabatic modification of the UTLS by the storm, and the presence of gravity waves and wavebreaking events introduces additional uncertainty to the inferred storm-top altitude. Spaceborne lidars and radars have been able to provide measurements of deep convection altitude (Setvák et al. 2013), but their narrow fields of view and sun-synchronous orbits lead to limited sampling and significant diurnal biases.

To understand the overall importance of deep tropopause-penetrating convection on the lower stratosphere, this study uses a new method introduced in Homeyer (2014) for combining reflectivities from individual Next Generation Weather Radar (NEXRAD) Weather Surveillance Radar-1988 Doppler (WSR-88D) sites into a three-dimensional composite with high vertical resolution to obtain storm-top altitudes. These altitudes are then compared with tropopause heights calculated from the ERA-Interim reanalysis to estimate the volume of air penetrating into the stratosphere. It is important to note that overshooting does not necessarily mean that all of the tropospheric air observed above the nominal tropopause altitude is irreversibly transported into the stratosphere. The term overshooting typically means that the convective plume has reached not only altitudes above the tropopause but also its own level of neutral buoyancy. As a result, much of the overshooting

air is likely to sink back into the troposphere. Irreversible transport into the stratosphere can occur, however, as a result of turbulent mixing on the boundary of the overshooting air, breaking gravity waves generated by the buoyant plume, or diabatic heating that increases the potential temperature of a parcel. The amount of irreversible transport will depend on the time scales of those processes relative to the period of the buoyancy oscillation of the overshooting air. The fraction of overshooting air that remains in the stratosphere (i.e., the transport efficiency) is poorly known. Thus, the volume of overshooting is likely substantially larger than the irreversible TST. Accurate quantitative transport estimates will require in situ observations of appropriate tracers and high-resolution numerical modeling, both of which pose significant challenges.

A second difficulty in making quantitative observations of overshooting convection is the relatively short time scales for convective plumes extending above the tropopause. Elliott et al. (2012) state: “The period of an OT [overshooting top] is wide ranging, with a lower limit of roughly 5 minutes and an upper limit of several hours. Generally, the strongest storms exhibit the largest OT diameters and the longest periods. It should be noted that long-lasting OTs are usually composed of numerous individual overshooting turrets which have much smaller diameters (<1 km) and smaller periods (1–2 min; Fujita 1974). These overshooting turrets are a result of updraft pulses lower in the storm. If the pulses occur frequently enough, the height of the OT may appear to remain relatively stationary, giving a false illusion that the updraft pulse remains constant through time.” A complete picture of overshooting convection will require higher-frequency sampling and better spatial resolution and would benefit from combining operational and research radar data with high-resolution, rapid-scan observations from geostationary satellites.

Here, we present a first step in creating a comprehensive observational database of overshooting convection through analysis of one year (2004) of NEXRAD reflectivity echoes above the tropopause over the continental United States east of the Rocky Mountains. To sample the diurnal cycle, the analysis is carried out at 3-h intervals. This will, therefore, underestimate the total number of overshooting events, but it should provide good estimates of the average instantaneous occurrence of overshoots during the diurnal and annual cycles and the geographical distribution of overshooting convection within the study area, as well as the vertical distribution of echo-top heights above the tropopause. Future studies will address the question of the lifetime of individual overshooting updrafts. An analysis of the relationship between overshooting

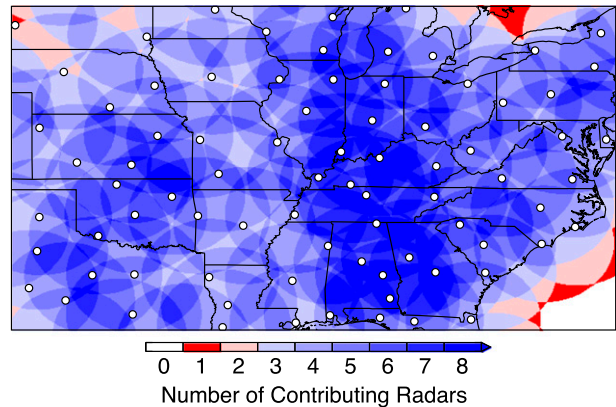


FIG. 1. The study area shows the number of NEXRAD units contributing to the gridded data at each point. Note that some of the radars used in the study are located outside the boundaries of the study region and are not shown on the map.

depth and the finescale structure of the tropopause is also given.

2. Data

a. NEXRAD WSR-88D data

The WSR-88D data used in this study (referred to herein as NEXRAD) are level-2 data files that were obtained from the National Climatic Data Center. NEXRAD units transmit a conical beam with an angular width of 0.95° . The nominal altitude of the beam increases with distance from the radar site as a result of the tilt of the radar and the curvature of the earth. Because of varying atmospheric refractive properties, beam position errors also generally increase with distance from the radar. The NEXRAD network was designed to ensure good coverage over densely populated areas (Leone et al. 1989). Because of these siting goals, coverage density generally decreases as you move west. For this study we use only radar sites located east of the Rocky Mountains. Figure 1 shows the locations and coverage of the NEXRAD units used in this study. When all of the radars are operating, most locations within the study area are observed by three or more overlapping radars, with a few exceptions near the boundary.

NEXRAD level-2 reflectivity data are used to determine echo-top altitudes. The level-2 data for 2004 from an individual radar are stored at a resolution of 1° in azimuth and 1 km in radial distance on a spherical grid. Elevation angles depend on the scanning mode in operation at a radar at a given time.

The sampling characteristics of a radar depend on several conditions including operating status, scan strategy, range of the target volume from the radar, and the current weather conditions around the radar site.

When there is convection in the vicinity of the site, the radar operates in “convective mode,” which makes a volume scan with 14 elevations every 5–8 min. The typical volume scan time in the absence of convection is ~10 min. For reflectivity the maximum effective measuring distance is 460 km (Crum and Alberty 1993). As outlined in section 1, we use data from a single year (2004). The large storage space required (5 TB yr⁻¹) and necessary computational time for both data download and processing contribute to this restriction.

b. ERA-Interim reanalysis

Tropopause heights are calculated by using atmospheric temperatures and geopotential heights from the interim version of the Interim European Centre for Medium-Range Weather Forecasts Re-Analysis (ERA-Interim). The reanalysis is produced with a sequential data assimilation scheme (Dee et al. 2011). Reanalysis data are available daily at 0000, 0600, 1200, and 1800 UTC on a global Gaussian grid with a resolution of ~0.75° latitude × 0.75° longitude and 37 unevenly spaced pressure levels in the vertical. The vertical resolution of the model output grid in the tropopause region is ~1 km.

c. Radiosonde data

Radiosonde data from stations within the study region are used to evaluate the quality of the tropopause heights calculated from the ERA-Interim analysis and to investigate the relationship between overshooting depth and physical characteristics of the tropopause. The radiosondes are operated by the National Weather Service (NWS) and launched from NWS sites around the country. The vertical resolution of each profile is ~30 m. In this study, 49 radiosonde stations located within the study region are used. Only radiosondes launched at 0000 UTC are included, resulting in a total of 13 437 comparison points.

3. Methods

Tropopause-penetrating convection is identified by the occurrence of NEXRAD echo tops that are higher than the collocated ERA-Interim tropopause. The altitude difference ΔZ , which is a function of longitude, latitude, and time, is defined as

$$\Delta Z = Z_e - Z_t, \quad (1)$$

where Z_e is the echo-top height and Z_t is the tropopause altitude. Overshooting is defined as any echo tops with $\Delta Z > 0$. That is, in this study we define overshooting tops as locations with radar reflectivity values ≥ 10 dBZ

that are above the large-scale lapse-rate tropopause. It is possible that the presence of a convective storm will increase the local altitude of the tropopause, but that cannot be determined from the available data, so we restrict our criteria to the use of large-scale analyzed tropopause height. It is important to note that, although the combined uncertainty of the echo-top altitude and tropopause altitude is ~1 km (see below), defining overshooting as $\Delta Z > 0$ helps to prevent the introduction of biases from using nonzero ΔZ thresholds, which may exclude real events and/or decrease the area of a storm identified as overshooting the tropopause.

The echo-top height Z_e is calculated from a three-dimensional reflectivity dataset created by combining data from individual radars into a regional composite. Compositing is done using the methods described in Homeyer (2014). For this analysis, composite reflectivities based on ~100 radar stations are calculated at eight daily synoptic times (0000, 0300, . . . , 2100 UTC) using the level-2 data that fall within ± 10 min of the analysis time. The study domain is the area from 30° to 45°N and from 75° to 103°W. Volume scans from each radar are interpolated from native spherical grids onto a regular 0.02° (~2 km) latitude–longitude grid, and then linearly interpolated to the 3-h synoptic analysis times using the two volume scans closest to each analysis time. Composite reflectivity profiles at each horizontal grid point are created by sorting the data from all available radars in altitude and then interpolating onto a regular vertical grid with a resolution of 1 km. Figure 3 in Homeyer (2014) shows that if at least three radars contribute to sampling a column, the vertical sampling interval for that column is less than or equal to 1 km. Therefore, to ensure accuracy, echo-top heights are estimated only where at least three contributing radars sample a column. Additionally, as shown by Homeyer (2014), the sensitivity of radar detection decreases as range from the radar increases. The maximum distance from the radar used for compositing is 300 km. At this distance the minimum detectable reflectivity is ~7.5 dBZ, so a threshold of 10 dBZ is used to determine the echo-top height for each column. Comparisons of the 10-dBZ echo-top altitude from the radar composite with higher-resolution satellite-based profiler observations reveal altitude uncertainties of ~500 m in the NEXRAD composite echo top (e.g., see Fig. 6 in Homeyer 2014).

ERA-Interim data are interpolated in space and, if necessary, in time in order to calculate tropopause heights at the temporal and spatial resolution of the composite radar files. For hours that fall during the ERA-Interim analysis times (0000, 0600, 1200, and 1800 UTC), the tropopause height is computed by first

interpolating the temperature and geopotential height horizontally in space to the $0.02^\circ \times 0.02^\circ$ composite radar grid. Each temperature column is then interpolated to a vertical resolution of 100 m using cubic splines. The World Meteorological Organization (WMO) definition (WMO 1957) is applied to determine primary and secondary tropopause locations as outlined in Homeyer et al. (2010). Several studies have shown that the WMO tropopause is closely tied to the chemical transition between the troposphere and stratosphere (Pan et al. 2004, 2007; Gettelman et al. 2011). To calculate the tropopause height for the intermediate times (0300, 0900, 1500, and 2100 UTC), the temperature and geopotential height are interpolated linearly to the desired analysis time before following the above procedure. The altitude difference ΔZ is then computed using Eq. (1). The data to be analyzed thus consist of 3-hourly maps of ΔZ for all of 2004.

4. Results

a. Tropopause calculation validation

To evaluate the accuracy of tropopause heights estimated from the ERA-Interim reanalysis, the ERA-Interim tropopause is compared with tropopause heights calculated from high-resolution radiosonde (also referred to as sondes) profiles. Radiosonde tropopause heights are calculated following the WMO definition as described in section 3. The ERA-Interim tropopause height is interpolated to the location of the sonde launch site and the heights from the two different sources are compared. Figure 2 shows that $\sim 77\%$ of heights agree within ± 0.5 km, and $\sim 91\%$ of points agree within ± 1 km (comparable to the vertical resolution of the model).

There are two distinct populations of points present in Fig. 2. The bulk of the points lie close to the 1-to-1 line; a second group contains points with ERA-Interim tropopause heights that are significantly higher than the radiosonde calculated values (ellipse in Fig. 2). These occur primarily where the radiosonde tropopause height is 12 km or higher. The occurrence of this second population of points has been previously documented in comparisons of tropopause heights from the NCEP Global Forecast System (GFS) with radiosonde data. Figure 4 of Homeyer et al. (2010) compares GFS tropopause heights with radiosonde data and shows a distribution of points very similar to what is found here. Homeyer et al. (2010) showed that these points are primarily due to the lower vertical resolution of the gridded analysis relative to the original radiosonde data. Because the vertical resolution of the radiosonde data is

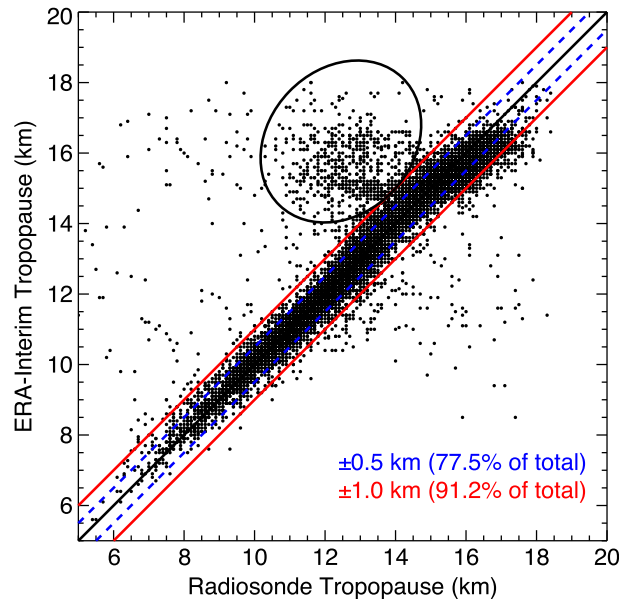


FIG. 2. Comparison of tropopause altitudes computed from radiosondes and from the ERA-Interim reanalysis. Points between the red lines are values that agree within ± 1 km. Points between the dashed blue lines are values that agree within ± 0.5 km. The ellipse is explained in text.

very high, incorrect tropopause identification with the sonde data is unlikely. The reanalysis fields, on the other hand, provide a smoothed version of the actual atmospheric temperature profiles. In some cases, particularly near the subtropical jet, the smoothed temperature profile in the gridded field does not satisfy the WMO definition near the true primary tropopause, and the secondary tropopause is erroneously identified as the primary tropopause. These misidentifications are more likely to occur where the change in stability from the troposphere to the stratosphere is relatively small or in cases where a secondary tropopause exists, which happens when there is a deep layer of low-stability air located some distance above the primary tropopause. Neglecting points within the ellipse in Fig. 2, $\sim 81\%$ of points agree within ± 0.5 km and $\sim 96\%$ of points are within ± 1 km. Note that perfect agreement is not to be expected because of model error and limited model resolution, instrument errors, and mismatches in the time and location of the comparison due to horizontal drift of the sonde as it rises, as well as the timing of the actual tropopause crossing.

Although the circled group of points in Fig. 2 does not make up a large portion of the total population ($\sim 6\%$), they are of interest for several reasons. Recent modeling and observational studies (Homeyer et al. 2014a,b) have shown that some of the deepest-penetrating convective storms occur in locations with a double tropopause. Failure to correctly identify the primary tropopause will

overestimate the tropopause height (Z_t) and underestimate the overshooting depth (ΔZ), which would lead to underestimation of the frequency of tropopause-penetrating convection. Examining locations where overshooting occurred within 250 km of a radiosonde site, double tropopauses were detected by sonde measurements $\sim 67\%$ of the time. The ERA-Interim calculation of tropopause height detected double tropopauses only $\sim 47\%$ of the time in the same locations. These tropopause misidentifications occur throughout the study area, but are most prevalent in the southern portion of the domain.

We investigate the impact of missed primary tropopauses on the statistics of overshooting by extracting a sample of collocated overshooting-radiosonde observations where the sonde tropopause is between 11 and 15 km and the ERA-Interim tropopause is at least 1 km higher. This results in a set of 641 soundings. In this set, 0.084% of the radar grid points have echo tops that overshoot the sonde tropopause, but not the ERA-Interim tropopause. We compare this with a random set of 641 soundings where the sonde tropopause is also between 11 and 15 km, but the difference between the tropopause heights is less than 1 km. In this set of soundings, only 0.019% of the radar grid points have echo tops that overshoot the sonde tropopause but not the ERA-Interim tropopause, a factor of about 4.4 smaller. Overshooting is most likely to occur in locations with weak lower-stratospheric stability or double tropopauses. These are also situations where the ERA-Interim is likely to miss the primary tropopause because of the inevitable smoothing of the temperature profile by the relatively coarse vertical grid of the reanalysis. Therefore, undiagnosed overshooting events are more likely to occur where the ERA-Interim tropopause misses the primary tropopause than in randomly selected cases.

The true fraction of overshooting events can be expressed as $f = (n_c + n_m)/N$, where n_c is the number of overshooting events where the tropopause is correctly identified, n_m is the number of overshooting events where the tropopause is misidentified, and N is the total number of analysis times, which can also be represented as $N_c + N_m$ (following the notation for occurrences of overshooting). Assuming that we detect all overshooting events when the tropopause is correctly identified and miss all of the events when the tropopause is misidentified, the fraction that is actually measured is $f = n_c/N$. Based on Fig. 2, however, $N_m \approx 0.06N_c$, so we can use the error factor computed from the collocated radiosonde-radar analysis to estimate n_m (i.e., $(n_m/N_m) = 4.4$, so $n_m = 4.4 \times 0.06 \times n_c = 0.26n_c$). Based on this, we estimate that we miss about $0.26/(1 + 0.26) \approx 20\%$ of the overshooting events due to missing the

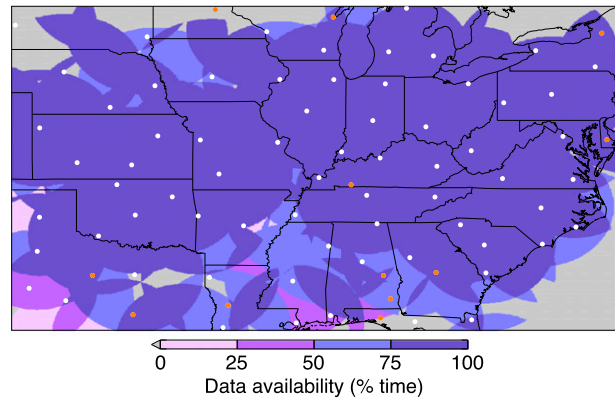


FIG. 3. Shading indicates the percentage of time that each point in the study domain has at least three radars sampling its column. Gray areas are regions where the column is not sampled by three or more radars at any time during the year. White dots denote radar locations with data available during the study period; orange dots denote radar locations with no data available throughout the study period.

primary tropopause and using a tropopause height that is too high.

b. Radar coverage

Because the radar data coverage is irregular in both space and time, we first assess how well the composited NEXRAD observations sample the study area. Figure 3 shows the percentage of time each location in the study area is sampled by at least three radars. The actual radar coverage over the study domain shown in Fig. 3 differs from what is shown in Fig. 1 for several reasons: 1) a contribution of at least three radars in a column is required for the echo-top estimate, 2) data from several stations are unavailable for the entire year, and 3) data availability changes throughout the year as a result of radar operating status and data archiving issues. Individual station locations (dots) are color coded in Fig. 3 based on their data availability. Stations in orange have no data available throughout the entire study period, and stations in white have data available for at least part of the study period. Coverage is best in an east-west zone across the center of the study area. There are several radars in the Southeast and Texas for which no data are available throughout the study period, resulting in coverage of 75% or less across parts of this region. Coverage along the northern boundary of the region is also lacking for the same reason. In the remainder of this paper, the occurrence of tropopause-penetrating convection is expressed as a percentage of the maximum possible area covered by three or more radars, which we designate as A_{\max} , where A_{\max} is the total area covered by observations from at least three radars at some time during the study period (i.e., nongray regions in Fig. 3).

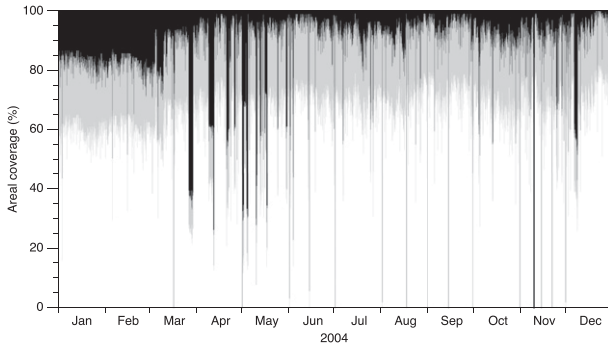


FIG. 4. Fraction of the study area in percent covered by four or more radars (white), by three radars (gray), and by two or fewer radars (black) as a function of time. Points within the rectangular study domain that are never sampled by three or more radars are excluded from this calculation.

We determine that $A_{\max} = 3.78 \times 10^6 \text{ km}^2$, which is $\sim 89\%$ of the total area of the map in Fig. 3.

Data availability also changes with time as a result of operational and data archiving issues. Changes in radar operating status are quite common and occur irregularly throughout the study period. No stations operated continuously throughout the study. Because many locations are observed by more than three radars, however, the loss of a single radar does not necessarily mean that a tropopause-penetrating convective event will go undetected. Figure 4 shows data availability for 2004 as a percentage of A_{\max} . At each 3-hourly observing time, white indicates the fraction of A_{\max} covered by four or more radars, gray is the fraction covered by three radars, and black is the fraction covered by two or fewer radars. These always sum to 100%. Approximately 65% of the study area is sampled by four or more radars throughout the study period. Coverage by three or more radars (the minimum needed for a reliable echo-top estimate) is near 90% throughout the year, with fluctuations as individual radar sites come on and off line and occasional short gaps for the entire network. The uptick in coverage starting in the middle of March is due to a return to operational status by several radars in the southern portion of the study area.

To ensure that coverage variations do not bias our estimates of the diurnal cycle of overshooting convection, we also examine the percent coverage by three or more overlapping radars as a function of time of day (not shown). Percent coverage at each 3-hourly analysis time is nearly constant, with values ranging between 82% and 89%, with no obvious systematic diurnal cycle in data availability.

c. Analysis

Figure 5 is an example of instantaneous maps of radar reflectivity and ΔZ for 0000 UTC 13 June 2004. On this

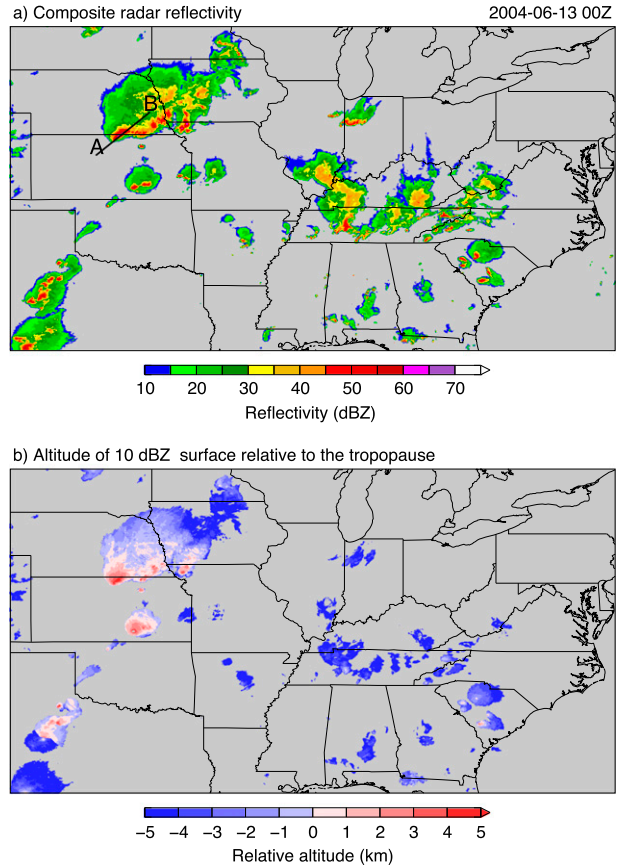


FIG. 5. Maps of (a) maximum radar reflectivity in each column (dBZ) and (b) altitude of the 10-dBZ surface relative to the tropopause (ΔZ) at 0000 UTC 13 Jun 2004. Line A–B in (a) marks the location of the cross section in Fig. 6, below.

day there are several deep convective systems present within the study area, some penetrating 4–5 km above the tropopause. This particular map has the largest total area of overshooting of any 3-h sample during the year. Figure 6 is a vertical cross section through the deep convection occurring near the Kansas–Nebraska border (line segment labeled A–B in Fig. 5). Colors indicate reflectivity; black lines denote the primary and secondary tropopauses. In this example convection has penetrated ~ 5 km above the primary tropopause, and, in some locations, ~ 1 km above the secondary tropopause. Examples of similarly deep storms have been reported in Homeyer et al. (2014b, their Figs. 1 and 13) and in Homeyer and Kumjian (2015, their Fig. 8). Supercells, and other types of storms in double-tropopause environments, are associated with large overshooting heights in those analyses. Although the focus of this study is on the statistical characteristics of overshooting convection, it is worth noting that the high vertical resolution of the composite product allows detailed observation of individual storms. The radar compositing

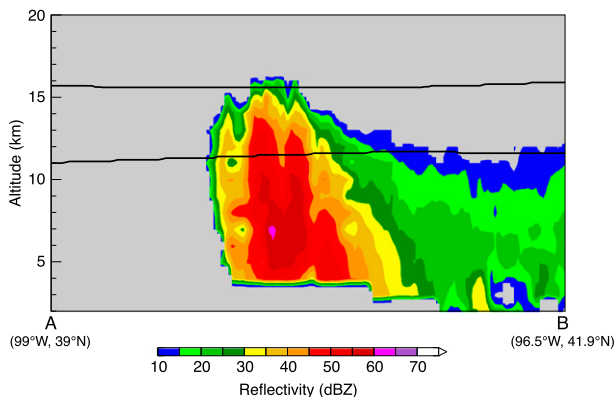


FIG. 6. Radar reflectivity cross section along the line A–B shown in Fig. 5. Black lines are the ERA-Interim primary and secondary tropopause.

method is therefore also useful for studying storm structure and related smaller-scale phenomena.

Figure 7 shows the occurrence of echo tops above the tropopause for each 3-h analysis time throughout 2004. Although the largest amount of total overshooting occurs in May of this year, Fig. 7 shows that the largest single event occurs in June and that much of each month's total occurs as the result of several large individual events. Figure 8 shows the cumulative 3-hourly occurrence of convection reaching the tropopause as a function of month. A strong annual cycle can be seen, with a distinct peak in the late spring and early summer months. These results are consistent with the annual cycles of the occurrence of deep convection, which is more common in the warm season, and of tropopause height, which increases through the summer (Wong and Wang 2000).

The geographical pattern of total tropopause-penetrating convection occurrence over the year is shown in Fig. 9. This map counts the number of 3-h analysis times during 2004 that each location experiences a reflectivity of 10 dBZ that reaches the level of the tropopause or higher. Figure 9 shows that overshooting convection events are most common over the high plains, particularly in Nebraska and Kansas, and infrequent east of the Mississippi River. There are very few occurrences of overshooting detected in the southeastern portion of the United States. Note that although Fig. 5b suggests regions of the storm top much larger than the deepest tropopause-penetrating elements are frequently classified as overshooting in our methods, distributions of overshooting at higher tropopause-relative thresholds consistent with observed convective lifting of the tropopause (e.g., >1 km) are qualitatively similar to that shown here. This result disagrees with the 5-yr climatology using satellite IR data

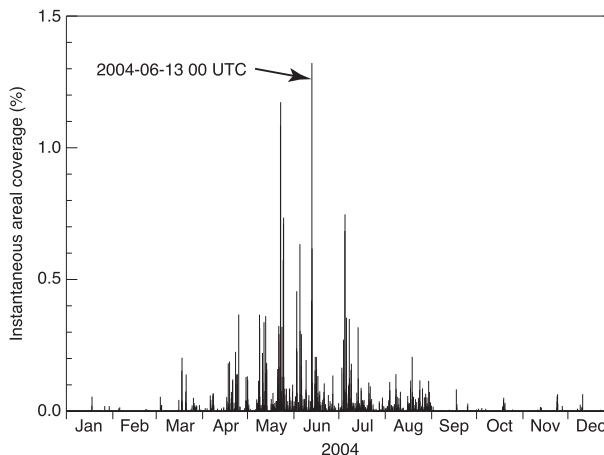


FIG. 7. Time series of occurrence of tropopause-penetrating convection as a percent of A_{\max} . Each vertical black line corresponds to one 3-hourly analysis. The analysis time shown in Figs. 5 and 6 is indicated by the label.

given in Bedka et al. (2010), which found a distinct maximum of overshooting convection in the Southeast. The reason for the discrepancy between these methods is not fully understood, but is likely related to the screening methods used in Bedka et al. (2010) for retaining observations where the cloud-top temperature is colder than the tropopause (see outline in section 1). Bedka et al. (2010) show the distribution of IR observations colder than the tropopause that were not retained for analysis (their Fig. 13). The geographic distribution of these events, which are classified by their algorithm as “nonovershooting cold pixels,” closely resembles the distribution of overshooting occurrences seen in Fig. 9 of this study. It is also notable that the discarded cold IR pixels in Bedka et al. (2010) were observed about 5 times as often as those retained for

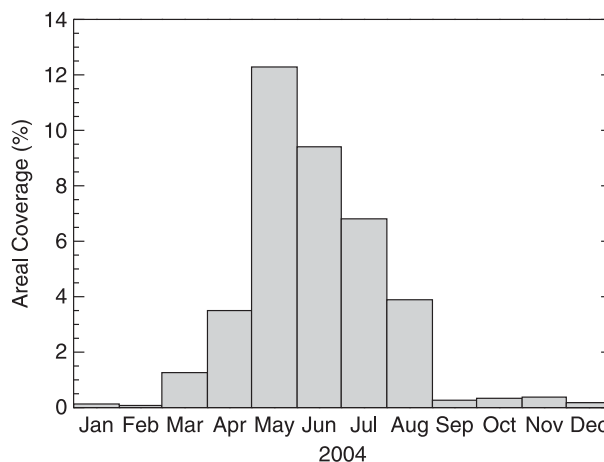


FIG. 8. Monthly cumulative areal coverage relative to A_{\max} .

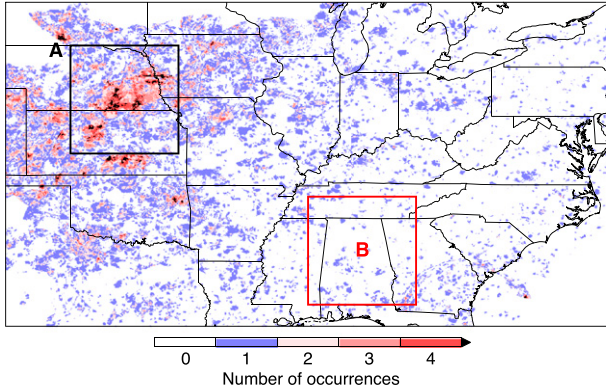


FIG. 9. Number of occurrences during 2004 of reflectivities ≥ 10 dBZ above the tropopause.

analysis. The omission of these cases may explain a large part of the discrepancy between the two analyses.

To determine why there are few occurrences of overshooting in the southeastern region of the United States, we examine histograms of storm-top and tropopause height in the high plains and Southeast regions (labeled A and B in Fig. 9). Figure 10 shows histograms of tropopause height (dashed lines) and height of the 10-dBZ surface (solid lines) in 1-km bins. Black lines are plotted for the high plains region (A), and red lines are for the southeastern region (B). Counts are done for the period of April–August. The average tropopause height in region A is several kilometers lower than that in region B, while the 10-dBZ surface reaches higher altitudes more often in region A than B. These distributions imply that overshooting is less likely in the Southeast because of both shallower storms and higher tropopause heights. Note also that Bedka et al.’s detection algorithm uses a brightness temperature threshold of 215 K to identify potential overshooting tops. This condition is met more frequently in regions like the southeastern United States, where overall cloud-top brightness temperatures are lower because of the higher and colder tropopause. In addition, the requirement that overshooting features in Bedka et al. (2010) be 6.5 K colder than the surrounding anvil temperatures may be more routinely met in storms where the equilibrium level (and altitude of the broader anvil) is well below the tropopause, which occurs more often when the tropopause altitude is high (>15 km). This would allow for storms that marginally exceed the altitude of the tropopause to be counted more frequently in the satellite observations.

Figure 11 shows the total annual occurrence of radar reflectivities of at least 10 dBZ that reach the level of the primary tropopause or higher as a function of time of day, expressed as a percentage of A_{\max} . Because the study area spans 28° of longitude, the local time varies by

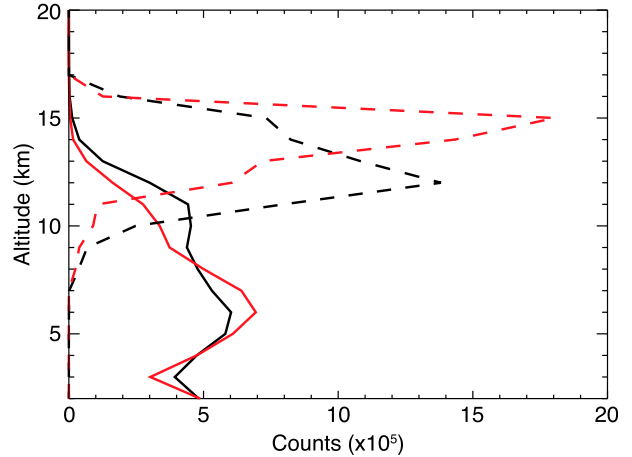


FIG. 10. Counts of tropopause height (dashed lines) and 10-dBZ echo top (solid lines) for high plains region A (black) and southeastern region B (red) in Fig. 9. Counts are for the months of April–August.

about ± 1 h from the synoptic analysis time, which for this region is about 6 h behind UTC. A strong diurnal cycle is present, with the highest likelihood of tropopause-penetrating events occurring around 0000 UTC (~ 1800 LT) and the lowest likelihood occurring around 1500 UTC (~ 0900 LT). This generally agrees with the observed diurnal cycle of midlatitude continental precipitation (Dai et al. 1999).

Figure 12 is an estimate of the total volume of air over the year that reaches different altitude levels above the tropopause based on the 3-hourly samples. This is computed by taking the storm-top-relative altitude (ΔZ) and multiplying it by the associated column area. The total volume of overshooting decreases rapidly as a function of height above the primary tropopause. It is important to note that, as with the cumulative area plot

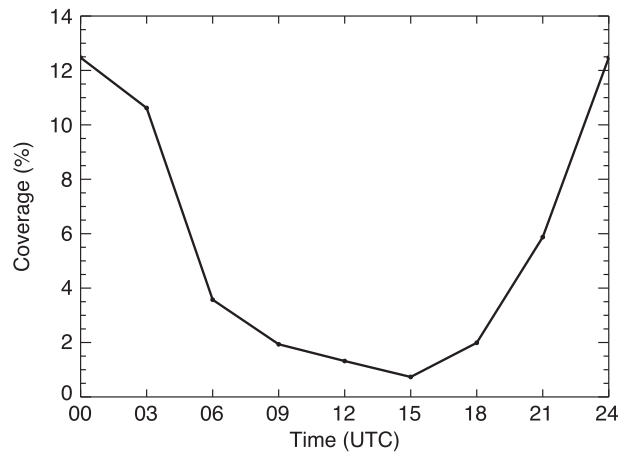


FIG. 11. Diurnal cycle of overshooting expressed as the percentages at each 3-hourly observing time summed over the year.

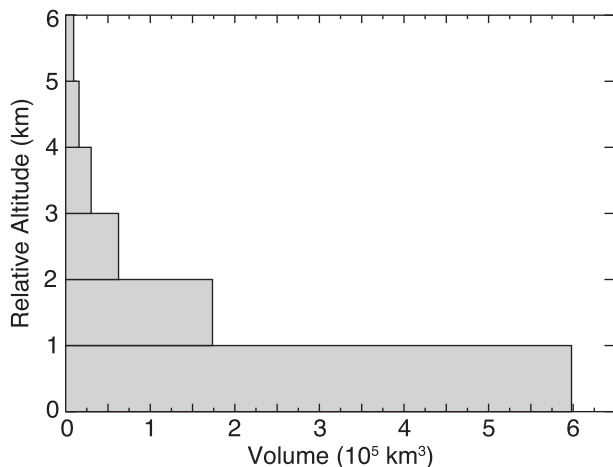


FIG. 12. Total volume of overshooting during 2004 as a function of altitude relative to the tropopause.

(Fig. 7), the total volume of overshooting is also dependent on the temporal resolution of the data.

d. Overshooting depth and tropopause characteristics

As outlined in section 4a, we find that with the ERA-Interim data, the secondary tropopause can be misidentified as the primary tropopause in double-tropopause environments, leading to increased potential for unidentified overshooting events and/or underestimation of the overshooting depth. In addition, the radiosonde–NEXRAD collocations in section 4a revealed that two-thirds of all overshooting events occur within double-tropopause environments, which suggests that overshooting is more likely in such cases. Motivated by this result and the recent arguments for deeper overshooting in double-tropopause environments than in single-tropopause cases presented in Homeyer et al. (2014a,b), we once again employ the collocated radiosonde–NEXRAD overshooting observations in this section in order to investigate the potential link between tropopause structure, lower-stratosphere stability, and overshooting depth in the radar composites.

It can be argued that at least two characteristics of the tropopause region can impact the depth of convective penetration into the lower stratosphere: 1) the sharpness of the tropopause and 2) the stability of the stratosphere above the tropopause inversion layer (or TIL). The TIL is broadly defined as the increase in stability and temperature with height occurring within the first 3 km above the tropopause (e.g., Birner et al. 2002; Birner 2006). The sharpness of the tropopause is often measured using the depth and “strength” of the TIL, where the depth is simply the distance from the tropopause to the level of maximum stability in the lowest 3 km of the stratosphere and the strength is represented by either

TABLE 1. Number of overshooting grid points and physical characteristics of the TIL associated with the primary tropopause from collocated radiosonde and NEXRAD observations. Data are provided for single- (ST) and double-tropopause (DT) environments.

| Type | No. of grid points | TIL depth (km) | TIL lapse rate ($-\Delta T/\Delta z$) ($K km^{-1}$) |
|------|--------------------|----------------|---|
| ST | 35 535 | 1.48 | −3.76 |
| DT | 73 393 | 0.74 | −4.32 |

the change in stability between the tropopause and the maximum or the mean lapse rate for the same layer (e.g., Schmidt et al. 2005; Wang and Polvani 2011). Table 1 provides the mean TIL depth and strength as measured by the lapse rate ($-\Delta T/\Delta z$) from the radiosonde observations for convective overshooting events within single-tropopause and double-tropopause environments. These parameters reveal that the TIL is stronger in double-tropopause environments, but half as deep as that in single-tropopause environments. Despite being stronger in double-tropopause cases, the reduced depth of the temperature (and stability) inversion and consequently lower negative buoyancy experienced by a parcel rising above the TIL implies that it would take longer for an ascending plume to decelerate when crossing the primary tropopause and TIL in a double-tropopause environment. As a result, the depth and likelihood of convective overshooting would be greater in double-tropopause environments.

Figures 13 and 14 demonstrate the observed relationship between the tropopause environment and overshooting depth using the entire radiosonde–NEXRAD dataset. In Fig. 13, frequency distributions of overshooting depth are given for both single-tropopause and double-tropopause environments. The double-tropopause environments are separated into those with mean lapse rates between the primary and secondary tropopauses (TPLR) that are tropospheric according to the WMO tropopause definition (i.e., $-\Delta T/\Delta z > 2 K km^{-1}$; red line) and those that are stratospheric (green line). These distributions reveal that overshooting is deeper in double-tropopause environments than in single-tropopause environments regardless of lower stratospheric stability, with the deepest overshooting events occurring in double-tropopause environments where the stability of the lower stratosphere is lowest (i.e., more tropospheric). This finding supports the argument that overshooting depth is sensitive both to tropopause sharpness and the stability of the lower stratosphere above the TIL. Figure 14 provides an alternative demonstration of the relationship between overshooting depth and lower stratosphere stability, where the mean overshooting depth is shown as a

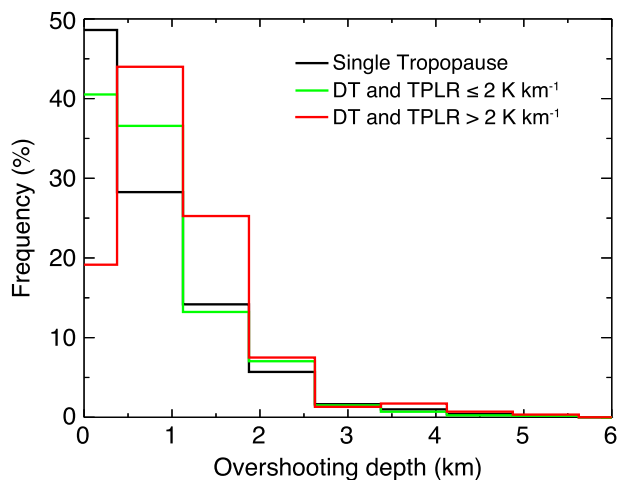


FIG. 13. For radiosonde–NEXRAD collocations, frequency distributions of overshooting depth for single-tropopause environments (black line), double-tropopause (DT) environments with the mean lapse rate between the primary and secondary tropopauses (TPLR) less than or equal to 2 K km^{-1} (green line), and DT environments with $\text{TPLR} > 2 \text{ K km}^{-1}$ (red line).

function of the TPLR for select double-tropopause environments (those with Δz between tropopauses ranging from 3.5 to 5 km). The comparison shows that the mean overshooting depth increases gradually as the lower stratosphere stability decreases (TPLR increases) from that similar to a single-tropopause environment to that hypothesized to deepen convective overshooting in [Homeyer et al. \(2014a,b\)](#).

5. Summary

This study uses a new method of compositing individual NEXRAD WSR-88D stations onto a regional grid with high horizontal and vertical resolution in order to diagnose the frequency, magnitude, and location of tropopause-penetrating convection events. Tropopause altitudes estimated from the ERA-Interim reanalysis show good agreement with high-resolution NOAA radiosonde data. In about 5% of cases within the study area, the ERA-Interim data fail to represent the primary tropopause, probably because of the limited vertical resolution. This results in the secondary tropopause being incorrectly identified as the primary tropopause, with the consequence that some storms that penetrate the tropopause may not be identified as such.

For 2004 the NEXRAD network provides good areal coverage, with at least three radars available throughout most of the study area. Despite fluctuations of radar coverage during the study period, there are no obvious sampling biases that would affect the

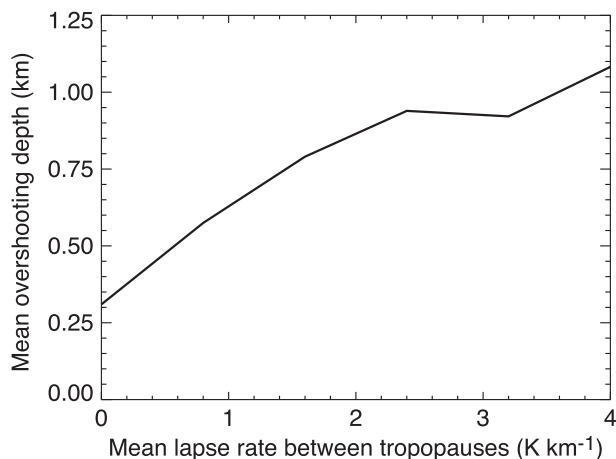


FIG. 14. For radiosonde–NEXRAD collocations, mean overshooting depth as a function of the TPLR for DT environments with depths between the primary and secondary tropopauses ranging from 3.5 to 5 km.

estimates of the diurnal or annual cycles. Reduced coverage in some areas in the southern part of the study region also does not appear to have caused systematic errors.

Analysis of instantaneous gridded radar fields and prior comparison with satellite observations (e.g., Fig. 6 in [Homeyer 2014](#)) shows that the compositing method works well and generates accurate regional reflectivity fields. In one case analyzed in detail, a cross section through a deep convection event reveals reflectivities of 10 dBZ penetrating ~ 5 km above the primary tropopause and 1 km above the secondary tropopause. Events of this magnitude are relatively rare during 2004. The lifetime of overshooting events can be as short as 5–15 min ([Bedka et al. 2010](#)), so analysis at higher frequency would likely increase the number of large events detected by the network. Future expansion of this analysis to additional years and higher time resolution will reduce sampling errors and allow study of interannual variability of the frequency and geographic distribution of overshooting events.

There is a distinct annual cycle in both the frequency and magnitude of overshooting events. The area of overshooting reaches a peak during May and is small from September to February. The largest individual event occurred in June. Single, large events make up a significant portion of each month's total percent area of overshooting. Occurrence maps show that tropopause-penetrating convection is most common during 2004 over the high plains and infrequent east of the Mississippi. The lack of occurrences in the Southeast differs significantly from the

findings of a 5-yr climatology performed by Bedka et al. (2010). That study also identified a large number of points colder than the tropopause that were not classified as overshooting by their algorithm but whose distribution of occurrence closely matches ours. A strong diurnal cycle is present with a peak around 0000 UTC and a minimum at 1500 UTC, which matches the well-known diurnal cycle of convection over the United States.

An assessment of the total volume of overshooting convection as a function of relative altitude shows that many of the storms identified as overshooting reach less than 1 km above the tropopause and the amount of overshooting volume falls off rapidly with increasing relative altitude.

Collocated observations of high-resolution radiosonde profiles and the NEXRAD composites were used to perform an analysis of the physical relationship between overshooting convection and tropopause structure. Comparison of single- and double-tropopause environments reveals clear dependencies of overshooting depth on the sharpness of the tropopause and the stability of the lower stratosphere above the tropopause inversion layer. This result supports arguments presented recently in modeling and aircraft case studies of deep convective overshooting within double-tropopause environments (Homeyer et al. 2014a,b).

Compositing individual radars into a single regional grid provides a high quality three-dimensional field of radar reflectivity. The coverage over the study domain is generally good, and suffers only in areas where NEXRAD sites are nonoperational for long periods of time. Further work is planned to extend the analysis to a longer time period and to higher temporal resolution in order to assess the interannual variability of overshooting convection events and to construct a long-term climatology. Other studies using this NEXRAD compositing method are also under way using the dual-polarization upgrade to the NEXRAD network in order to examine storm structure in detail (e.g., Homeyer and Kumjian 2015).

Acknowledgments. This research was funded by NSF Grant AGS-1016191 to Texas A&M University. Author CH was supported in part by the Advanced Study Program at the National Center for Atmospheric Research (NCAR). NCAR is sponsored by the National Science Foundation. The authors thank all of the producers, archivers, and distributors of the data used in the study. The radar data were obtained in 2013 from the NEXRAD Data Archive at the NOAA/National Climatic Data Center (<https://www.ncdc.noaa.gov/nexradinv/>). The

ERA-Interim reanalysis is produced by the European Centre for Medium-Range Weather Forecasts. Data files were obtained from the NCAR Data Support Section (<http://rda.ucar.edu/datasets/ds627.0/>). Radiosonde data are taken from the NOAA/ESRL Radiosonde database (<http://www.esrl.noaa.gov/raobs/>).

REFERENCES

- Ackerman, S. A., 1996: Global satellite observations of negative brightness temperature differences between 11 and $6.7\ \mu\text{m}$. *J. Atmos. Sci.*, **53**, 2803–2812, doi:10.1175/1520-0469(1996)053<2803:GSOONB>2.0.CO;2.
- Adler, R. F., M. J. Markus, and D. D. Fen, 1983: Thunderstorm top structure observed by aircraft overflights with an infrared radiometer. *J. Climate Appl. Meteor.*, **22**, 579–593, doi:10.1175/1520-0450(1983)022<0579:TTSOBA>2.0.CO;2.
- Alcala, C. M., and A. E. Dessler, 2002: Observations of deep convection in the tropics using the Tropical Rainfall Measuring Mission (TRMM) precipitation radar. *J. Geophys. Res.*, **107**, 4792, doi:10.1029/2002JD002457.
- Anderson, J. G., D. M. Wilmouth, J. B. Smith, and D. S. Sayres, 2012: UV dosage levels in summer: Increased risk of ozone loss from convectively injected water vapor. *Science*, **337**, 835–839, doi:10.1126/science.1222978.
- Bedka, K., J. Brunner, R. Dworak, W. Feltz, J. Otkin, and T. Greenwald, 2010: Objective satellite-based detection of overshooting tops using infrared window channel brightness temperature gradients. *J. Appl. Meteor. Climatol.*, **49**, 181–202, doi:10.1175/2009JAMC2286.1.
- Berendes, T. A., J. R. Mecikalski, W. M. MacKenzie Jr., K. M. Bedka, and U. S. Nair, 2008: Convective cloud identification and classification in daytime satellite imagery using standard deviation limited adaptive clustering. *J. Geophys. Res.*, **113**, D20207, doi:10.1029/2008JD010287.
- Bigelbach, B. C., G. L. Mullendore, and M. Starzec, 2014: Differences in deep convective transport characteristics between quasi-isolated strong convection and mesoscale convective systems using seasonal WRF simulations. *J. Geophys. Res. Atmos.*, **119**, 11 445–11 455, doi:10.1002/2014JD021875.
- Birner, T., 2006: Fine-scale structure of the extratropical tropopause. *J. Geophys. Res.*, **111**, D04104, doi:10.1029/2005JD006301.
- , A. Dörnbrack, and U. Schumann, 2002: How sharp is the tropopause at midlatitudes? *Geophys. Res. Lett.*, **29**, 1700, doi:10.1029/2002GL015142.
- Chagnon, J. M., and S. L. Gray, 2010: A comparison of stratosphere–troposphere transport in convection-permitting and convection-parameterizing simulations of three mesoscale convective systems. *J. Geophys. Res.*, **115**, D24318, doi:10.1029/2010JD014421.
- Crum, T. D., and R. L. Alberty, 1993: The WSR-88D and the WSR-88D Operational Support Facility. *Bull. Amer. Meteor. Soc.*, **74**, 1669–1687, doi:10.1175/1520-0477(1993)074<1669:TWATWO>2.0.CO;2.
- Dai, A., F. Giorgi, and K. E. Trenberth, 1999: Observed and model-simulated diurnal cycles of precipitation over the contiguous United States. *J. Geophys. Res.*, **104**, 6577–6402, doi:10.1029/98JD02720.
- Dee, D. P., and Coauthors, 2011: The ERA-Interim reanalysis: Configuration and performance of the data assimilation

- system. *Quart. J. Roy. Meteor. Soc.*, **137**, 553–597, doi:10.1002/qj.828.
- Dessler, A. E., 2002: The effect of deep, tropical convection on the tropical tropopause layer. *J. Geophys. Res.*, **107**, 4033, doi:10.1029/2001JD000511.
- Dickerson, R. R., and Coauthors, 1987: Thunderstorms: An important mechanism in the transport of air pollutants. *Science*, **235**, 460–465, doi:10.1126/science.235.4787.460.
- Elliott, M. S., D. R. MacGorman, T. J. Schuur, and P. L. Heinselman, 2012: An analysis of overshooting top lightning mapping array signatures in supercell thunderstorms. *Proc. 22nd Int. Lightning Detection Conf.*, Broomfield, CO, Vaisala. [Available online at <http://www.vaisala.com/en/events/ildcilmc/archive/Pages/ILDC-2012-archive.aspx>.]
- Fischer, H., and Coauthors, 2003: Deep convective injection of boundary layer air into the lowermost stratosphere at midlatitudes. *Atmos. Chem. Phys.*, **3**, 739–745, doi:10.5194/acp-3-739-2003.
- Forster, P., and Coauthors, 2007: Changes in atmospheric constituents and in radiative forcing. *Climate Change 2007: The Physical Science Basis*, S. Solomon et al., Eds., Cambridge University Press, 129–234.
- Fritz, S., and I. Laszlo, 1993: Detection of water vapor in the stratosphere over very high clouds in the tropics. *J. Geophys. Res.*, **98**, 22 959–22 967, doi:10.1029/93JD01617.
- Fromm, M. D., and R. Servranckx, 2003: Transport of forest fire smoke above the tropopause by supercell convection. *Geophys. Res. Lett.*, **30**, 1542, doi:10.1029/2002GL016820.
- Fujita, T. T., 1974: Overshooting thunderheads observed from ATS and Learjet. University of Chicago Dept. of the Geophysical Sciences Satellite and Mesometeorology Research Project Research Paper 117, 29 pp. [Available online at <http://ntrs.nasa.gov/archive/nasa/casi.ntrs.nasa.gov/19740018973.pdf>.]
- Gottelman, A., M. L. Salby, and F. Sassi, 2002: Distribution and influence of convection in the tropical tropopause region. *J. Geophys. Res.*, **107**, 4080, doi:10.1029/2001JD001048.
- , P. Hoor, L. L. Pan, W. J. Randel, M. I. Hegglin, and T. Birner, 2011: The extratropical upper troposphere and lower stratosphere. *Rev. Geophys.*, **49**, doi:10.1029/2011RG000355.
- Gray, S. L., 2003: A case study of stratosphere to troposphere transport: The role of convective transport and the sensitivity to model resolution. *J. Geophys. Res.*, **108**, 4590, doi:10.1029/2002JD003317.
- Hanisco, T. F., and Coauthors, 2007: Observations of deep convective influence on stratospheric water vapor and its isotopic composition. *Geophys. Res. Lett.*, **34**, L04814, doi:10.1029/2006GL027899.
- Hegglin, M. I., and Coauthors, 2004: Tracing troposphere-to-stratosphere transport above a mid-latitude deep convective system. *Atmos. Chem. Phys.*, **4**, 741–756, doi:10.5194/acp-4-741-2004.
- Holton, J. R., P. H. Haynes, M. E. McIntyre, A. R. Douglass, R. B. Rood, and L. Pfister, 1995: Stratosphere–troposphere exchange. *Rev. Geophys.*, **33**, 403–439, doi:10.1029/95RG02097.
- Homeyer, C. R., 2014: Formation of the enhanced-V infrared cloud-top feature from high-resolution three-dimensional radar observations. *J. Atmos. Sci.*, **71**, 332–348, doi:10.1175/JAS-D-13-079.1.
- , and M. R. Kumjian, 2015: Microphysical characteristics of overshooting convection from polarimetric radar observations. *J. Atmos. Sci.*, **72**, 870–891, doi:10.1175/JAS-D-13-0388.1.
- , K. P. Bowman, and L. L. Pan, 2010: Extratropical tropopause transition layer characteristics from high-resolution sounding data. *J. Geophys. Res.*, **115**, D13108, doi:10.1029/2009JD013664.
- , L. L. Pan, and M. C. Barth, 2014a: Transport from convective overshooting of the extratropical tropopause and the role of large-scale lower stratosphere stability. *J. Geophys. Res.*, **119**, 2220–2240, doi:10.1002/2013JD020931.
- , and Coauthors, 2014b: Convective transport of water vapor into the lower stratosphere observed during double tropopause events. *J. Geophys. Res. Atmos.*, **119**, 10 941–10 958, doi:10.1002/2014JD021485.
- Leone, D. A., R. M. Endlich, J. Petričeks, R. T. H. Collis, and J. R. Perter, 1989: Meteorological considerations used in planning the NEXRAD network. *Bull. Amer. Meteor. Soc.*, **70**, 4–13, doi:10.1175/1520-0477(1989)070<0004:MCUIPT>2.0.CO;2.
- Lindsey, D. T., and L. Grasso, 2008: An effective radius retrieval for thick ice clouds using GOES. *J. Appl. Meteor. Climatol.*, **47**, 1222–1231, doi:10.1175/2007JAMC1612.1.
- Martin, D. W., R. A. Kohrs, F. R. Mosher, C. M. Medaglia, and C. Adamo, 2008: Over-ocean validation of the global convective diagnostic. *J. Appl. Meteor. Climatol.*, **47**, 525–543, doi:10.1175/2007JAMC1525.1.
- Mullendore, G. L., D. R. Durran, and J. R. Holton, 2005: Cross-tropopause tracer transport in midlatitude convection. *J. Geophys. Res.*, **110**, D06113, doi:10.1029/2004JD005059.
- Negri, A. J., 1982: Cloud-top structure of tornado storms on 10 April 1979 from rapid scan and stereo satellite observations. *Bull. Amer. Meteor. Soc.*, **63**, 1851–1859.
- Pan, L. L., W. J. Randel, B. L. Gary, M. J. Mahoney, and E. J. Hintsa, 2004: Definitions and sharpness of the extratropical tropopause: A trace gas perspective. *J. Geophys. Res.*, **109**, D23103, doi:10.1029/2004JD004982.
- , and Coauthors, 2007: Chemical behavior of the tropopause observed during the stratosphere-troposphere analyses of regional transport experiment. *J. Geophys. Res.*, **112**, D18110, doi:10.1029/2007JD008645.
- Poulida, O., R. R. Dickerson, and A. Heymsfield, 1996: Stratosphere-troposphere exchange in a midlatitude mesoscale convective complex: 1. Observations. *J. Geophys. Res.*, **101**, 6823–6836, doi:10.1029/95JD03523.
- Ray, E. A., and Coauthors, 2004: Evidence of the effect of summertime midlatitude convection on the subtropical lower stratosphere from CRYSTAL-FACE tracer measurements. *J. Geophys. Res.*, **109**, D18304, doi:10.1029/2004JD004655.
- Rosenfeld, D., W. L. Woodley, A. Lerner, G. Kelman, and D. T. Lindsey, 2008: Satellite detection of severe convective storms by their retrieved vertical profiles of cloud particle effective radius and thermodynamic phase. *J. Geophys. Res.*, **113**, D04208, doi:10.1029/2007JD008600.
- Schmetz, J., S. A. Tjemkes, M. Gube, and L. van de Berg, 1997: Monitoring deep convection and convective overshooting with METEOSAT. *Adv. Space Res.*, **19**, 433–441, doi:10.1016/S0273-1177(97)00051-3.
- Schmidt, T., S. Heise, J. Wickert, G. Beyerle, and C. Reigber, 2005: GPS radio occultation with CHAMP and SAC-C: Global monitoring of thermal tropopause parameters. *Atmos. Chem. Phys.*, **5**, 1473–1488, doi:10.5194/acp-5-1473-2005.
- Setvak, M., R. M. Rabin, and P. K. Wang, 2007: Contribution of the MODIS instrument to observations of deep convective storms and stratospheric moisture detection in GOES and MSG imagery. *Atmos. Res.*, **83**, 505–518, doi:10.1016/j.atmosres.2005.09.015.
- , K. Bedka, D. T. Lindsey, A. Sokol, Z. Charvátka, J. St’astka, and P. K. Wang, 2013: A-Train observations of deep convective storm tops. *Atmos. Res.*, **123**, 229–248, doi:10.1016/j.atmosres.2012.06.020.
- Stohl, A., H. Wernli, P. James, M. Bourqui, C. Forster, M. A. Liniger, P. Seibert, and M. Sprenger, 2003: A new perspective

- of stratosphere–troposphere exchange. *Bull. Amer. Meteor. Soc.*, **84**, 1565–1573, doi:[10.1175/BAMS-84-11-1565](https://doi.org/10.1175/BAMS-84-11-1565).
- Wang, P. K., 2003: Moisture plumes above thunderstorm anvils and their contributions to cross-tropopause transport of water vapor in midlatitudes. *J. Geophys. Res.*, **108**, 4194, doi:[10.1029/2002JD002581](https://doi.org/10.1029/2002JD002581).
- Wang, S., and L. M. Polvani, 2011: Double tropopause formation in idealized baroclinic life cycles: The key role of an initial tropopause inversion layer. *J. Geophys. Res.*, **116**, D05108, doi:[10.1029/2010JD015118](https://doi.org/10.1029/2010JD015118).
- WMO, 1957: Meteorology—A three-dimensional science: Second session of the Commission for Aerology. *WMO Bull.*, **IV** (4), 134–138.
- Wong, S., and W.-C. Wang, 2000: Interhemispheric asymmetry in the seasonal variation of the zonal mean tropopause. *J. Geophys. Res.*, **105**, 26 645–26 659, doi:[10.1029/2000JD900475](https://doi.org/10.1029/2000JD900475).